Table S1. Bacterial strains, plasmids and primers used in this study.

| Bacteria, plasmid or primer | Genotype/ Characteristics | Reference |
|---|---|---|
| **Bacteria strains** | | |
| *Salmonella enterica* Typhimurium JOL2500 | Δ*lon*, Δ*cpxR*, Δ*sifA*, Δ*asd* | (41) |
| *Escherichia coli* DH5α | F– φ80lacZΔM15 Δ(lacZYA-argF)U169 recA1 endA1 hsdR17(rK–, mK+) phoA supE44 λ– thi-1 gyrA96 relA1 | Lab stock |
| **Plasmids** | | |
| pcDNA3.2 | Vector backbone for eukaryotic expression | Lab stock |
| pcDNA3.2::Pept#1 | Vector carrying Pept#1 ORF | This study |
| pcDNA3.2::Pept#2 | Vector carrying Pept#2 ORF | This study |
| pcDNA3.2::Pept#3 | Vector carrying Pept#3 ORF | This study |
| pcDNA3.2::Pept#4 | Vector carrying Pept#4 ORF | This study |
| **Primer** | | |
| *IFN-γ* FP | TCAAGTGGCATAGATGTGGAAGAA | Lab stock |
| *IFN-γ* RP | TGGCTCTGCAGGATTTTCATG | |
| *TNF-α* FP | CATCTTCTCAAAATTCGAGTGACAA | Lab stock |
| *TNF-α* RP | TGGGAGTAGACAAGGTACAACCC | |
| *IL-6* FP | GGAGGCTTAATTACACATGTT | Lab stock |
| *IL-6* RP | TGATTTCAAGATGAATTGGAT | |
| *IL-4* FP | ATCATCGGCATTTTGAACGAGGTC | Lab stock |
| *IL-4* RP | ACCTTGGAAGCCCTACAGACGA | |
| *β-actin* FP | AGAGGGAAATCGTGCGTGAC | Lab stock |
| *β-actin* RP | CAATAGTGATGACCTGGCCG | |

**Table S2.** The selected APR sequences for LDHA isoforms 1 and 2

| Type of LDHA | Fewer falls' positives | Best overall performance | High sensitivity | Selected |
|---|---|---|---|---|
| Isoform 1 | KDQLIVNLL<br>KLVIITA | KDQLIVNLL<br>KLVIITA<br>RNVNIFKFIIPNI<br>DILTYVAWKIS | KDQLIVNLLK<br>PQNKITV<br>MACAISILM<br>HGSLF<br>KLVIITA<br>RNVNIFKFIIPNI<br>CKLLIVSNPVDILTYVAWKISGF<br>AYEVIKLKGYTSWAIGLSV<br>LAESIMK<br>IKGLYGIN<br>DVFLSV<br>GQNGISDVVKVTLT<br>ADTLWGIQKELQF | KDQLIVNLL<br>KLVIITA<br>RNVNIFKFIIPNI<br>DILTYVAWKIS |
| Isoform 2 | TSVLFFHFK<br>KDQLIVNLL<br>KLVIITA<br>RNVNIFKFIIPNI<br>DILTYVAWKIS | TSVLFFHFK<br>KDQLIVNLL<br>KLVIITA<br>RNVNIFKFIIPNI<br>DILTYVAWKIS | GGYTYTETSVLFFHFK<br>KDQLIVNLLK<br>PQNKITV<br>MACAISILM<br>HGSLF<br>KLVIITA<br>RNVNIFKFIIPNI<br>CKLLIVSNPVDILTYVAWKISGF<br>AYEVIKLKGYTSWAIGLSV<br>LAESIMK<br>IKGLYGIN<br>DVFLSV<br>GQNGISDVVKVTLT<br>ADTLWGIQKELQF | TSVLFFHFK<br>KDQLIVNLL<br>KLVIITA<br>RNVNIFKFIIPNI<br>DILTYVAWKIS |

**Table S3.** Designed peptide sequences for APR therapeutic applications

| Name | Original Peptide Sequence | Designed Sequence | Length |
|---|---|---|---|
| Pept#1 | KLVIITA | WD KLVIITA D GS D KLVIITA D | 21 |
| Pept#2 | RNVNIFKFIIPNI | WD RNVNIFKFIIPNI D GS D RNVNIFKFIIPNI D | 33 |
| Pept#3 | DILTYVAWKIS | WDDILTYVAWKIS D GS D DILTYVAWKIS D | 29 |
| Pept#4 | KDQLIVNLL | WD KDQLIVNLL D GS D KDQLIVNLL D | 25 |

**Table S4.** Peptide's estimated physico-chemical properties

| Sequence | Number of residues | MW (g/mol) | Extinction coefficient (1/M.cm) | Iso-electric point | Net charge at pH7 | Estimated solubility |
|---|---|---|---|---|---|---|
| Pept#1 | 21 | 2286.62 | 5690 | 3.71 | -2 | Good |
| Pept#2 | 33 | 3948.48 | 56990 | 6.81 | 0 | Poor |
| Pept#3 | 29 | 3389.71 | 19630 | 3.41 | -4 | Good |
| Pept#4 | 25 | 2883.21 | 5690 | 3.41 | -4 | Good |

**Table S5.** Summary of comparative docking profiles of Pept#2 with mouse and human LDHA analyzed by HDOCK pipeline.

| Parameter | Mouse LDHA | Human LDHA |
|---|---|---|
| Primary structural interfaces | N-terminal tetramerization arm<br>APR flanking loop<br>Oligomerization arm | APR loop<br>C-terminal helix |
| Key LDHA interface domains | N-teminal arm : Gln20, Asn21<br>β-core/loop: residues 88-90, 129-132<br>Tetramer interface: 263-256, 297-299 | |
| N-terminal arm engagement | Direct strong binding<br>Asn21-Asn12: 2.36Å<br>Gln20-Asn12: 3.22 Å | None |
| Oligomerization interface engagement | Direct binding<br>Met264, Gln297, Asn298 | None |
| Shortest contact distance | Lys90 - Ile9 (1.668 Å)<br>Asn156 - Phe8 (2.050 Å)<br>Gln297 - Ile10 (2.254 Å)<br>Asn21 - Asn12 (2.363 Å) | Ile150 - Ile5 (2.088 Å)<br>Lys328 - Arg1 (2.711 Å)<br>Gln327 - Arg1 (2.866 Å) |
| Structural & biological consequence | Direct disruption of the N-terminal assembly arm and subunit interfaces, leading to tetramer destabilization and aggregation | Peripheral binding to C-terminal helix without destabilizing the N-terminal tetramerization arm |

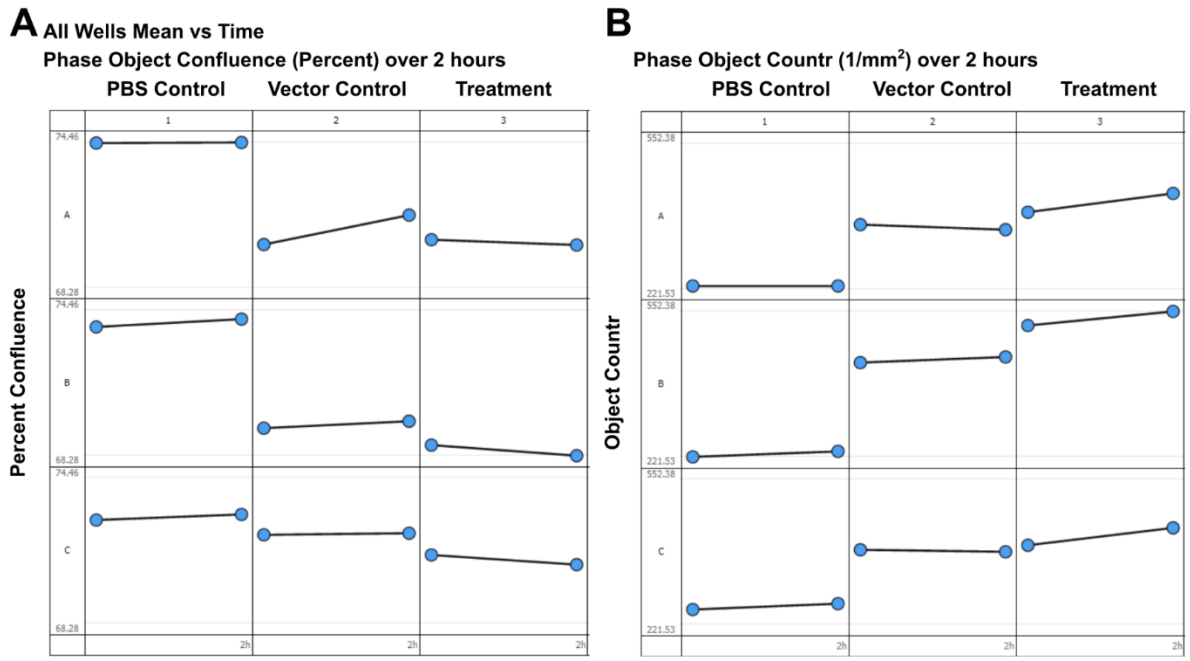


**Fig. S1.** Assessment of peptide-induced cytotoxicity and cell specificity. A metric analysis was conducted using the IncuCyte metric analysis module. (A) Phase object confluence and (B) Phase object counting was conducted.

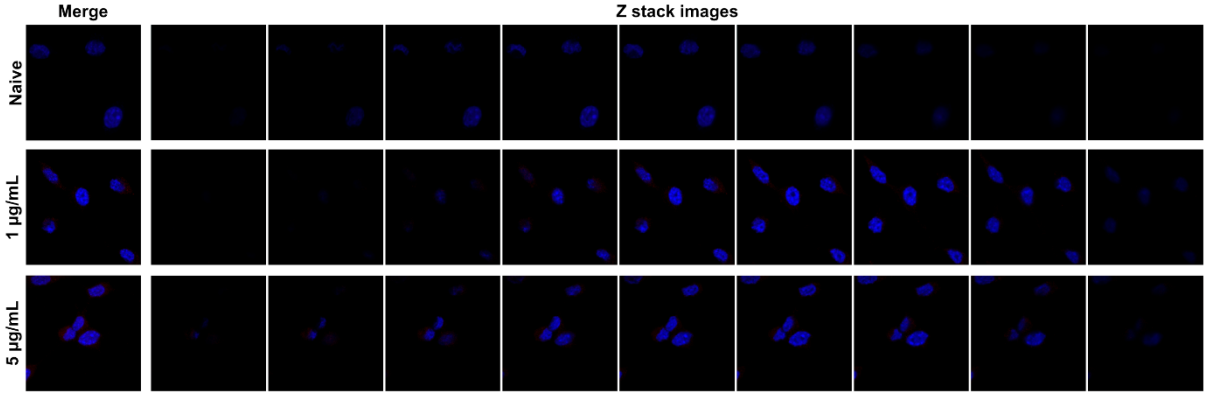


**Fig. S2** Fluorescence microscopy images of CT26 cells treated with FLAG-tagged Pept#2. Cells were treated with 0, 1, or 5 µg/mL of the peptide. Naïve cells (0 µg/mL) served as the negative control. Pept#2-treated cells exhibited a dose-dependent increase in red fluorescence, indicating successful cellular uptake of the non-encapsulated peptide. Imaging was performed using a confocal laser scanning microscope at 400× magnification. Z-stack images were acquired and processed into projections using ZEN software to confirm intracellular localization.

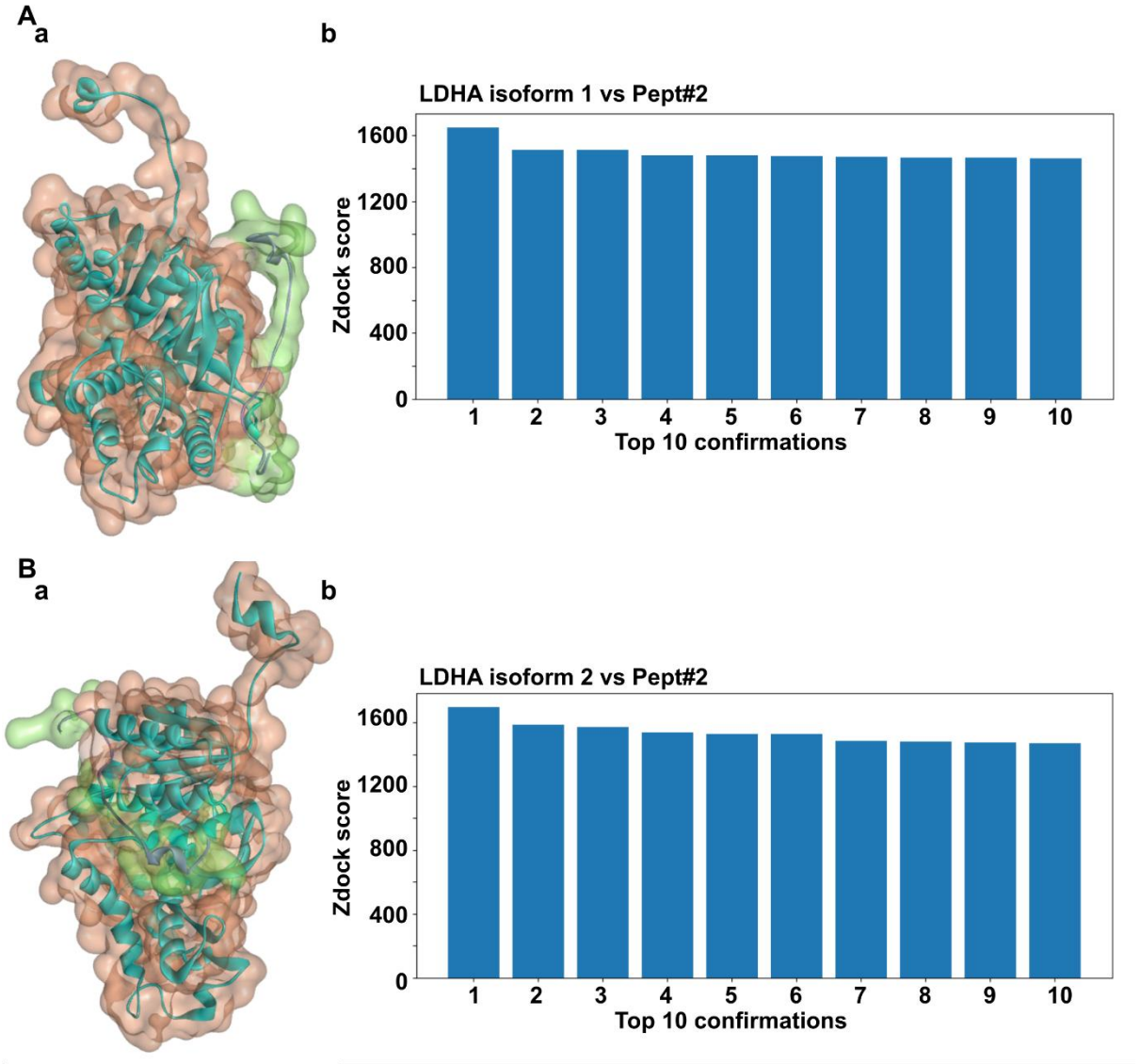


**Fig. S3** Docking assessment of mouse LDHA isoform 1 (A) and isoform 2 (B). Mouse isoform 1 and 2 sequences were retrieved from the NCBI database and modeled by submitting them to the SWISS Model server. By default, the auto-model algorithm was used to create each structure. The Pept#2 model was created using the Phyre2 server, modeled under intensive conditions. Protein and peptide docking was conducted on the Zdock server without specifying interaction residues. The best interaction pose between Pept#2 and LDHA isoform 1 (a) along with the top ten docking scores (b) are shown for both isoforms.

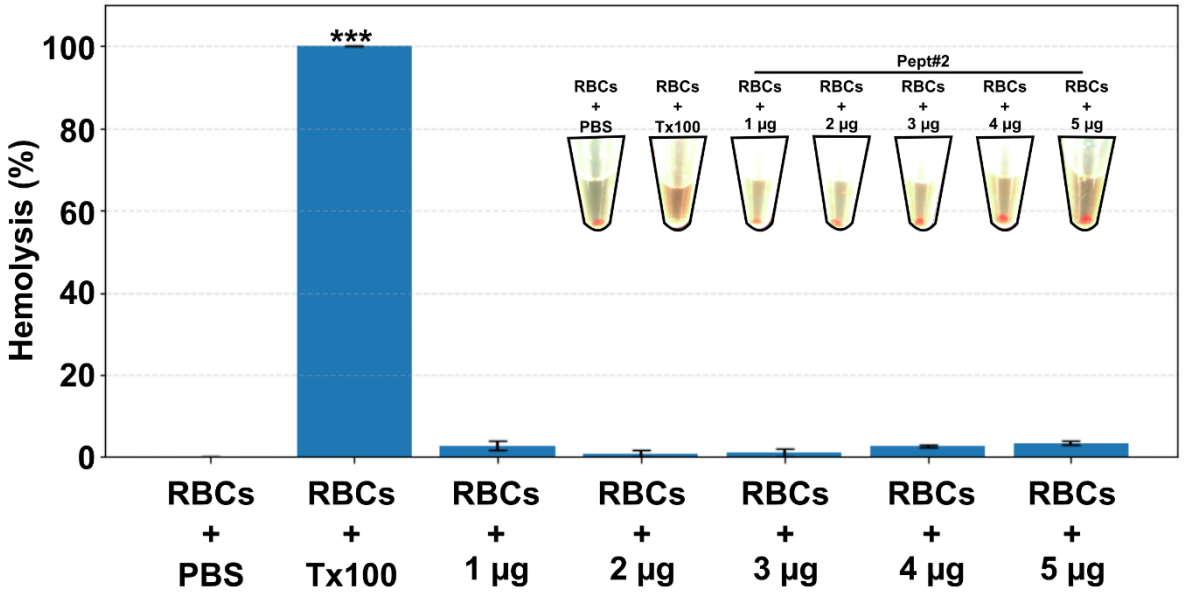


**Fig. S4** Pept#2 safety assessment by hemolysis. The hemolysis assay was conducted using defibrinated sheep blood with pure peptide Pept#2. Two percent sheep blood was prepared in PBS. The total of 400 µL reaction volumes were ready for PBS suspended RBCs, RBCs suspension supplemented with 0.1% Triton X-100 (Tx100) and increasing concentrations of Pept#2, 1 to 5 µg per reaction. Eppendorf tubes were mixed well and incubated for 1 hr. at 37 °C. Suspensions were subjected to slow centrifugation (1500 RPM) for 5 min, and the supernatants were collected for absorbance measurements at 540 nm in replicates. ***<0.001. The level of significance was determined at $p<0.05$.

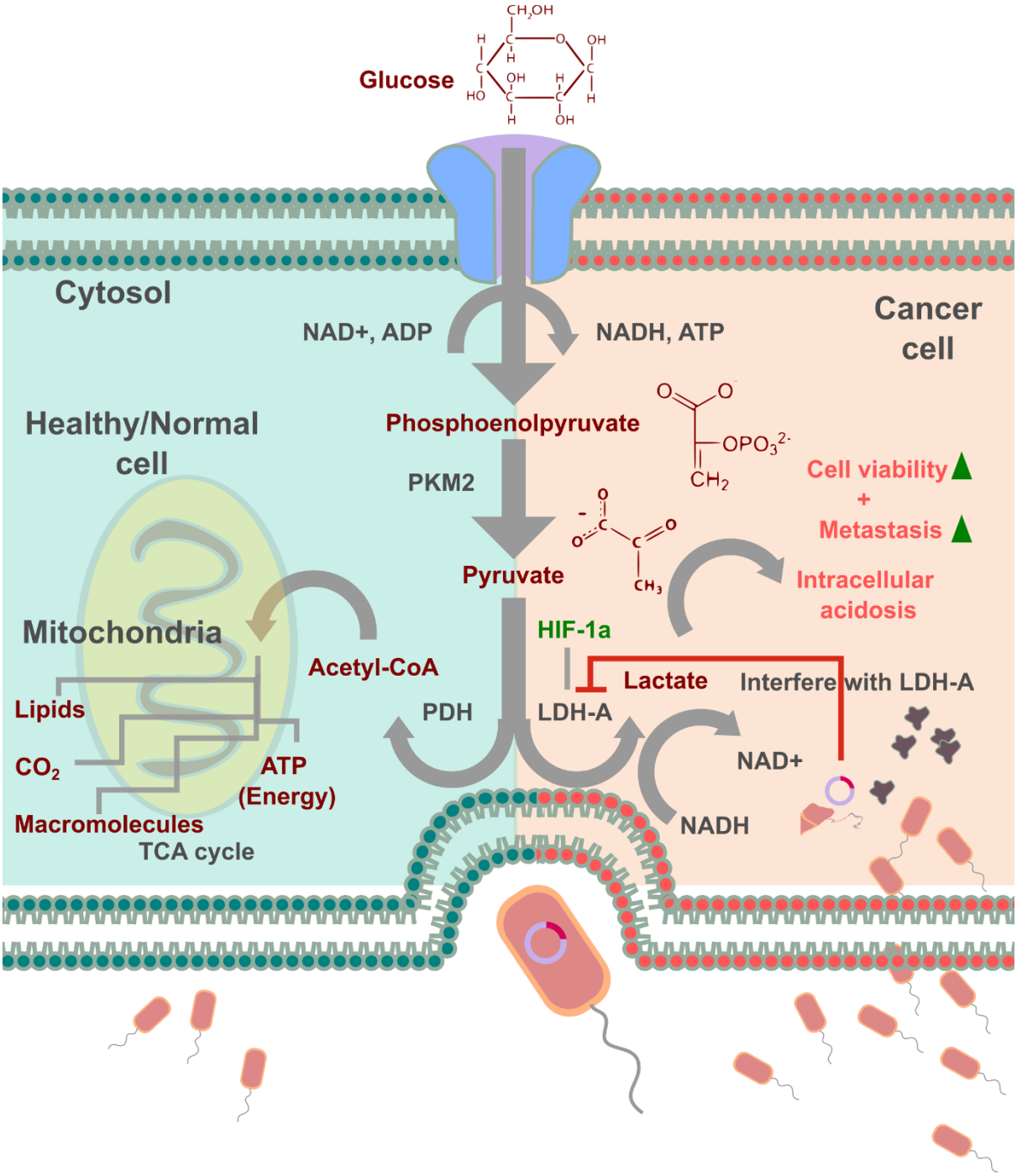


**Fig. S5** A schematic representation of how therapeutic peptides affect energy metabolism in cancer cells compared to a healthy scenario. Interference of LDHA functions abrogates energy and material flow for tumor growth and progression.

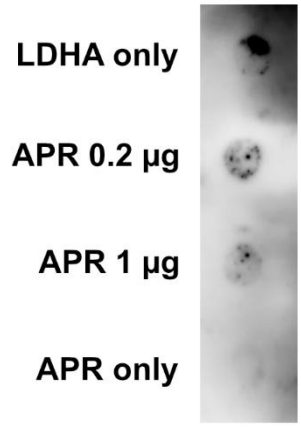


**Fig. S6** Dot blot analysis of Pept#2-mediated LDHA degradation. Purified LDHA (1 µg) protein was co-incubated with increasing concentrations of the APR peptide (Pept#2). The mixture was then spotted onto a nitrocellulose membrane, and intact LDHA was detected using an anti-LDHA antibody. The signal intensity of LDHA decreases in a dose-dependent manner as the concentration of the APR peptide increases, confirming the direct interaction and loss of soluble LDHA. The sample, APR only, serves as a negative control to ensure the anti-LDHA antibody does not cross-react with the peptide.

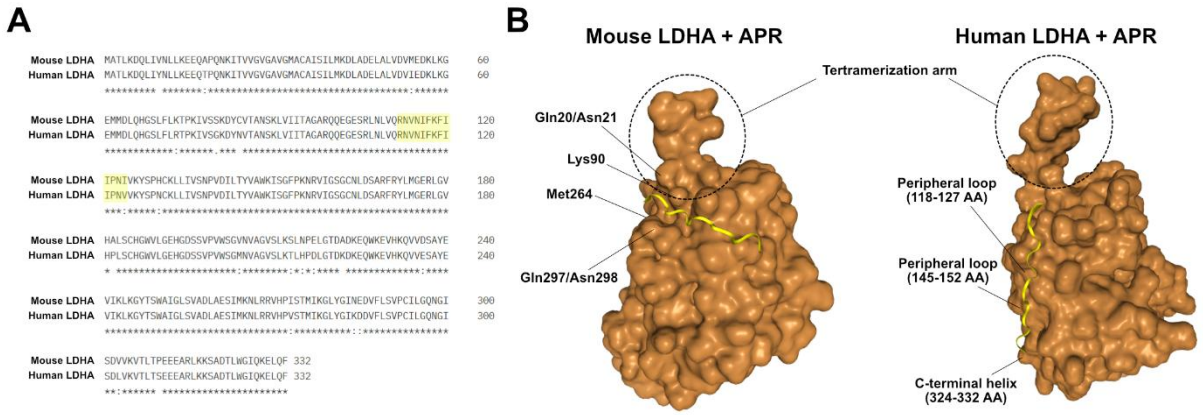


**Fig. 7S** Sequence alignment and comparative HDOCK molecular docking of APR sequence with mouse and human LDHA. (A) Amino acid sequence alignment of the LDHA sequences. Sequence alignment between mouse LDHA (UniProt P06151) and human LDHA (UniProt P00338). The 13-mer core APR sequences were highlighted (92.3% sequence identity). Asterisks indicate identical amino acids across the alignment and the colon denotes the single conservative aliphatic substitution at position 124 (I124 in mouse vs. V124 in human). (B) HDOCK structural model of Pept#2 interacting with mouse LDHA. Surface representation of the LDHA monomer complexed with the Pept#2 APR core (colored ribbon). Insets show detailed views of the interaction interface, demonstrating direct engagement with the N-terminal tetramerization arm (Gln20 at 3.22 Å and Asn21 at 2.36 Å/2.69 Å) as well as the internal and inter-subunit assembly residues (Lys90 at 1.67 Å, Met264, and Gln297/Asn298 at 2.25–2.72 Å). In human LDHA interactions, APR docks into an alternative peripheral surface encompassing the local APR loop (residues 118–127) and the C-terminal α-helix (Trp324–Phe332). The complete absence of contact with the N-terminal tetramerization arm (Gln20/Asn21) or the inter-subunit assembly hubs was noted, indicating a non-disruptive binding mode relative to the active tetrameric complex.